Quantum interference effects in molecular spin hybrids

Taner Esat,[1,2,3] Rico Friedrich,[4,3] Frank Matthes,[2,3] Vasile Caciuc,[4,3] Nicolae Atodiresei,[4,3] Stefan Blügel,[4,3] Daniel E. Bürgler,[2,3] F. Stefan Tautz,[1,3] and Claus M. Schneider[2,3]

[1]*Peter Grünberg Institute, Functional Nanostructures at Surfaces (PGI-3), Forschungszentrum Jülich, 52425 Jülich, Germany*

[2]*Peter Grünberg Institute, Electronic Properties (PGI-6), Forschungszentrum Jülich, 52425 Jülich, Germany*

[3]*Jülich Aachen Research Alliance (JARA), Fundamentals of Future Information Technology, 52425 Jülich, Germany*

[4]*Peter Grünberg Institute and Institute for Advanced Simulation, Quantum Theory of Materials (PGI-1/IAS-1), Forschungszentrum Jülich, 52425 Jülich, Germany*

We have studied by means of low-temperature scanning tunneling microscopy (STM) and spectroscopy (STS) single molecular spin hybrids formed upon chemisorbing a polycyclic aromatic, threefold symmetric hydrocarbon molecule on Co(111) nanoislands. The spin-dependent hybridization between the Co d states and the π orbitals of the molecule leads to a spin-imbalanced electronic structure of the chemisorbed organic molecule. Spin-sensitive measurements reveal that the spin polarization shows intramolecular variations among the different aromatic rings in spite of the highly symmetric adsorption geometry promoted by symmetry matching of the threefold symmetric molecule and the sixfold symmetric Co(111) lattice. Hence the varying degree of spin polarization on the organic molecule does not stem from a different hybridization of the aromatic rings with the Co atoms, but is proposed to be a consequence of the superposition of the spin polarization of the molecule and the spatially modulated spin polarization of the spin-dependent quantum interference pattern of the Co(111) surface state.

I. INTRODUCTION

In order to design miniaturized spin-based devices, e.g., for data storage, spintronics [1–4] or quantum computation [5–9], the interest in magnetic properties of nanostructures is currently in the focus of research. However, the precise design of magnetic nanostructures is a quite challenging task, since small changes, e.g., in the size, shape and composition, can lead to drastic changes of the magnetic properties, e.g., magnetic moments or switching fields [10–12].

The problems due to inhomogeneities could be avoided by using single-molecule magnets [13] with large magnetic moments and high magnetic anisotropy, since molecules can be synthesized in large numbers with identical properties. However, up to now such single-molecule magnets are limited to the operation at cryogenic temperatures, because thermal fluctuations can easily change the magnetization direction and/or magnitude at higher temperatures. Stabilizing the magnetization of a molecule by magnetic exchange coupling to a ferromagnetic building block is one possible solution for this problem [14–18]. An alternative approach is to tailor a hybrid molecular magnet from a nonmagnetic molecule by spin-dependent hybridization with a ferromagnetic building block. Besides the fact that the electronic and magnetic properties of the molecule are tuned, e.g., by inducing a magnetic moment or other spin-dependent features [19–21], also the magnetic properties of the ferromagnetic building block are affected [22]. Such effects can lead to magnetic hardening or softening of the newly formed unit consisting of the chemisorbed molecule and its direct metal neighbors [19,23,24]. Since such new hybrid systems promise unique magnetic functionalities, they are currently studied intensively [19,21,25–30].

The idea of this work is based on the latter approach, namely, on the spin-dependent hybridization of a nonmagnetic, aromatic molecule on a ferromagnetic surface. Here, the key is that the spin-dependent hybridization between the d states of the ferromagnetic metal and the π orbitals of the molecule leads to a spin-imbalanced electronic structure of the chemisorbed molecule [31,32]. Besides the question if it is possible to form such a hybrid molecular magnet, the main focus of this work is placed on the question if it is possible to have different spin-dependent effects, i.e., enhancement and inversion of the spin polarization in comparison to the polarization of the surrounding ferromagnetic surface, on the same molecule at the same time, for instance on different aromatic rings. To address this question and to find out, if it is possible to tailor a hybrid molecular magnet that exhibits varying spin features for different units, i.e., different aromatic rings, we have employed the molecule 2,4,6-triphenyl-1,3,5-triazine or shortly TPT shown in Fig. 1. TPT consists of a central triazinelike ring and three peripheral phenyl groups. In the gas phase, it is nonmagnetic and exhibits a threefold rotational symmetry. For the ferromagnetic building block, we haven chosen Co nanoislands on Cu(111), since this system has already been studied in detail and because it is known that its spin polarization is spatially modulated [33]. This makes the Co nanoislands an ideal system to investigate the spin-dependent hybridization and in particular to study the possibility to create a hybrid molecular magnet that may exhibit varying spin features for different units.

II. METHODS

A. Sample preparation

All measurements in this work have been carried out in a commercially available scanning tunneling microscope equipped with a Joule-Thomson cooling stage (JT-STM from SPECS) at a base temperature of $T = 4.3$ K and magnetic fields up to 3 T (out-of-plane) in ultrahigh vacuum (UHV) conditions. The Cu(111) crystal was prepared by repeated cycles of Ar$^+$ sputtering and subsequent annealing to 700 K
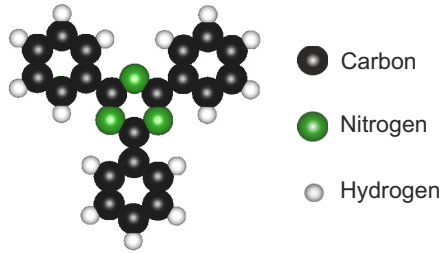
FIG. 1. Graphical representation of the 2,4,6-triphenyl-1,3,5-triazine (TPT) molecule in the gas phase.

for 10 minutes. In the next step, a submonolayer amount of Co [$\lesssim$0.4 monolayers (ML)] was deposited at a rate of $\approx$0.2 ML/min from a rod by electron bombardment heating onto the clean Cu(111) surface held at room temperature. This preparation procedure leads to the formation of triangular and 2-ML-high Co islands of varying sizes [34,35]. In order to minimize contaminations and also intermixing of Co and Cu atoms the sample was directly transferred into the STM [36]. The electronic and magnetic properties of the Co islands were checked by spin-polarized STM before the deposition of the TPT molecules. The TPT molecules were sublimated from a home-built Knudsen cell (deposition temperature approximately 415 K) onto the precooled sample ($\lesssim$70 K) to reduce the mobility of the adsorbed molecules. The coverage with TPT molecules was chosen such that typically less than four TPT molecules adsorbed per Co island. The pressure during the deposition of Co and the TPT molecules did not exceed 2×10^{-10} mbar.

B. Magnetic tip preparation

In order to investigate also the magnetic properties of the sample, a spin-sensitive STM tip is needed. Besides the obvious choice of ferromagnetic materials for the fabrication of the tips [37–39], antiferromagnetic materials can be used [40–42]. Antiferromagnetic materials have the advantage that they only exhibit weak stray fields, and an influence of the tip on the investigated magnetic structures can therefore be excluded, making them more suitable for small and magnetically susceptible structures. For this reason, we have used bulk Cr tips for our spin-sensitive measurements. Note that besides the use of bulk materials it is also possible to coat nonmagnetic STM tips with (anti)ferromagnetic materials [43–46].

The Cr tips have been fabricated by electrochemical etching of polycrystalline Cr rods in 5 M NaOH. The Cr rods have been obtained from a 99.95 % Cr foil. Before making use of the electrochemically etched bulk Cr tips they have been cleaned *ex situ* in distilled water and isopropanol and furthermore in UHV by electron bombardment heating (1 kV, 2.6 mA, 30 s) to remove the remaining oxides. Although it is known that the apex of the tip is likely spin-polarized, the direction of the tip magnetization, its strength and also the response to an external magnetic field are usually unknown [47]. Indeed, not all fabricated Cr tips showed the desired properties (high out-of-plane sensitivity) in the first instance. Therefore the Cr tips have also been treated *in situ* by applying short voltage pulses (4–10 V, 10 ms) between the STM tip and sample in order

to obtain appropriate magnetic tips. The magnetic sensitivity of the Cr tips has been checked by spectroscopic imaging of clean Co islands at different magnetic fields (see Sec. III A).

C. Differential conductance spectra and images

Differential conductance dI/dV spectra have been acquired using conventional lock-in technique with the feedback loop switched off. Parameters at the stabilization point before switching off the feedback loop were bias voltage $V = -200$ mV and tunneling current $I = 200$ pA. Spectroscopic maps of the first derivative dI/dV (dI/dV maps) have been measured simultaneously with constant-current images also using the conventional lock-in technique. The typical parameters were a modulation amplitude of 10 mV with a modulation frequency of 801 Hz. To ensure a featureless DOS of the tip, we measured reference spectra on the clean Cu(111) surface before starting measurements on the Co islands and TPT molecules. All differential conductance spectra shown in this work have been averaged over two measurements, one being a forward, the other a backward sweep of the bias voltage.

D. Theory

1. Computational details

Spin-polarized electronic structure calculations were carried out in the framework of density functional theory (DFT) [48,49] making use of the VASP program [50–52]. In addition, projector augmented-wave (PAW) data sets [53] as constructed for the Perdew, Burke, and Ernzerhof (PBE) exchange-correlation functional [54] were employed. Throughout the calculations a plane wave cutoff of 500 eV was used and the Brillouin zone was sampled at the Γ point. All structures were geometrically optimized until the forces were smaller than 10 meV/Å.

The unit cell was made up of two unfaulted fcc-stacked Co layers on top of five fcc-stacked Cu layers each represented by an 8×8 in-plane surface unit cell containing 64 Co or Cu atoms. The TPT molecule was adsorbed on top of the Co layers. The vacuum distance in the direction perpendicular to the surface plane to the next periodic slab was about 18 Å. The shortest lateral distance between two atoms of TPT molecules in neighboring unit cells was 8.8 Å. During the geometry optimization the uppermost Cu layer, the Co layers and the molecular coordinates were allowed to relax. Note that due to the periodic boundary conditions employed in our first principles calculations, it is not computationally tractable to investigate large Co nanoislands on Cu(111) to describe the Co(111) surface state interference effects as measured in the STM and STS experiments. Therefore, in the following, we will refrain from presenting a direct comparison between the calculated density of states and the measured dI/dV spectra.

2. Geometric structure

As depicted in Fig. 2, in the ground state, the TPT molecule adsorbs with its C atoms of the central triazine-like ring on top of the hcp hollow sites while the N atoms are over the surface Co ones. This adsorption position is consistent with both the experimental findings and the general tendency of N to adsorb on top of surface atoms [55]. Additionally, the calculated
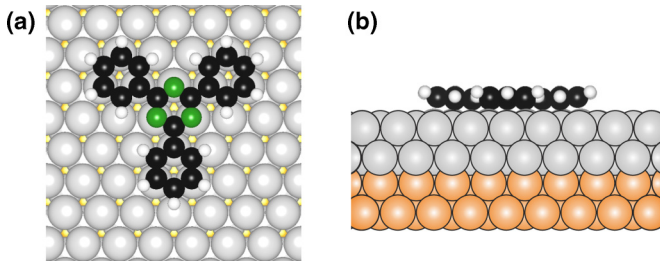
FIG. 2. Ground-state adsorption geometry of a single TPT molecule on 2-ML Co/Cu(111): (a) top view and (b) side view. Note that in this adsorption configuration the TPT molecule has the C atoms of the central ring on top of the hcp hollow sites and the N atoms above the Co surface atoms. Color code: Co (gray), Cu (orange), C (black), N (green), and H (light gray).

adsorption energy E_{ads} of 3.55 eV [56] clearly indicates that on 2-ML Co/Cu(111) the TPT molecule is chemisorbed. This conclusion is further supported by a N-Co distance of 2.07 Å and an average C-Co one of 2.06 Å for the Co atoms directly below the N and C ones, respectively.

As regarding the magnetic properties of the hybrid molecule-surface system, we first note that upon the TPT adsorption the magnetic moments of the twelve surface Co atoms underneath the molecule (three below each molecular ring) are modified. More specifically, due to the hybridization between these twelve surface Co atoms and the TPT molecule their magnetic moments are reduced compared to the clean surface moment of 1.8 μ_B. In a qualitative agreement with the results reported in Ref. [23], the Co moments below N of 1.6 μ_B are less diminished than the ones underneath C amounting to 1.4–1.5 μ_B. Besides this, with respect to the clean surface Co-Co inter-layer distance of 2.40 Å the average one for the hybrid TPT-surface is slightly larger (i.e., 2.43 Å). This observation implies that for this hybrid system a molecular-induced skyhook effect [24] is possible such that an inter-layer softening of the magnetic exchange interactions between the Co layers can occur.

III. RESULTS

A. Co islands on Cu(111)

In this section, the main properties of the Co island are only briefly introduced, since the growth, electronic and magnetic properties of this system have already been intensively investigated before [10–12,33,45,57–61].

Co islands prepared on the Cu(111) surface according to the procedure described in Sec. II A exhibit the typical triangular shape [inset of Fig. 3(a)] and bilayer height of approximately 3.9 Å. Two different orientations of the Co islands on the Cu(111) surface correspond to fcc (unfaulted) or hcp (faulted) stacking of the first Co layer with respect to the stacking of the substrate [35].

Figure 3(a) displays a typical dI/dV conductance spectrum, which has been acquired in the center of a Co island. The spectrum shows a sharp peak at approximately −330 mV, which corresponds to the spin-polarized d-like minority surface state of Co [59]. The broad peak at $\approx$+310 mV corresponds also to a spin-polarized d-like minority state [57,62].
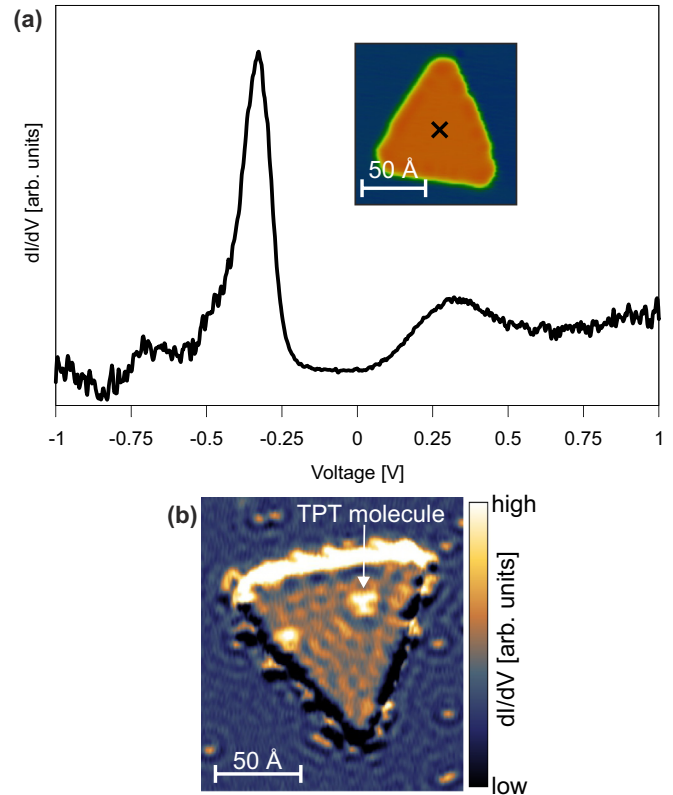

FIG. 3. (a) Differential conductance dI/dV spectra acquired in the center of a Co island. For the measurement, a nonmagnetic tungsten tip has been used. Inset shows the STM image of the corresponding Co island with the marked spectroscopy location ($V = 500$ mV and $I = 200$ pA). (b) dI/dV map of a Co island at $V = +690$ mV. The spatially modulated pattern is a result of the sp electron confinement in the Co island. A detailed analysis of the adsorption of the TPT molecules is presented in Sec. III B.

Furthermore, a free electron-like sp majority surface state with a parabolic dispersion starting around −0.17 V below the Fermi energy [33,59], which is not directly visible in the differential conductance spectra, because it is not a localized peak but smeared out over a broad energy range, can be visualized by measuring spectroscopic images. This is illustrated in Fig. 3(b), where a quantum inference pattern is clearly visible due to the scattering of the sp electron waves at the boundaries of the Co island. This quantum confinement gives rise to the observed standing waves. The interference pattern in Fig. 3(b) is measured at +0.69 V, i.e., well inside the existence range of the sp surface state that has been observed to extend up to +2.4 V [59]. The d-like surface state is not influenced by the electron confinement because of its energetically and spatially localized nature [63]. The spin polarization at a certain energy E is given by the difference of the density of states (DOS) of electrons with opposite spin at the given energy E normalized by the spin-integrated DOS at E. Note that the spatially modulated DOS of the sp surface state leads to a spatially modulated spin polarization across the Co islands [33]. This spatial modulation of the spin polarization is the key for understanding the magnetic properties of the TPT molecules reported in Sec. III D and discussed in Sec. IV.
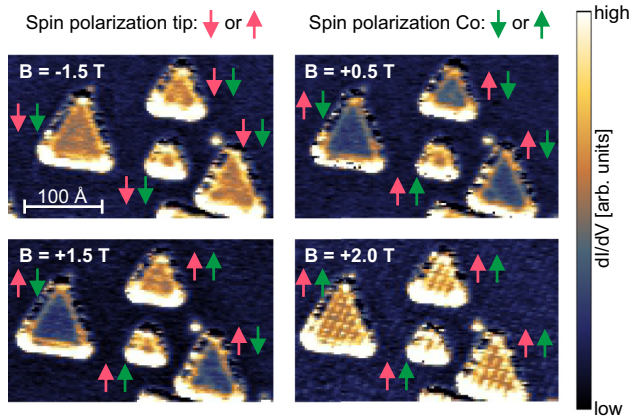
FIG. 4. dI/dV maps of Co islands on Cu(111) at different external magnetic fields B measured with a spin-polarized bulk Cr tip ($V = -500$ mV and $I = 1$ nA). Changes in the contrast correspond to the magnetization reversal of the tip ($B = +0.5$ T) or the Co islands ($B \geqslant +0.5$ T). The arrows next to the Co islands indicate the spin polarization of the tip and the particular Co island, respectively. The pattern in the spectroscopic image for $B = +2.0$ T is due to noise and not related to the standing waves within the Co island.

The electronic properties show no significant difference for faulted and unfaulted Co islands. Only the d-like surface state shifts slightly in energy (<50 mV) for differently oriented Co island as well as for different island sizes [60]. These small variations are specific for each Co island and, thus, necessitate that the spin-polarized measurements, namely for magnetically parallel and antiparallel configuration, must always be carried out on the same island and molecule, because otherwise the data are not comparable.

The Co islands exhibit an out-of-plane magnetization (parallel to the surface normal) and can be switched by an external magnetic field. In order to check the properties of the bulk Cr tip, we measured dI/dV maps of Co islands at a fixed bias voltage at different magnetic fields applied in the out-of-plane direction. Since the spin-polarized current and therefore also the differential conductance depends strongly on the relative orientation of the magnetization directions of the Co islands and the tip, a change in the magnetization is visible in the dI/dV signal, i.e., as a change in the contrast in the spectroscopic images. The results are shown in Fig. 4. At a magnetic field of $B = -1.5$ T, all Co islands have the same color. By changing the magnetic field to $B = +0.5$ T, the contrast of the Co islands (except the smallest one) is inverted from bright to dark. With further increase of the magnetic field at first one Co island changes its contrast from dark to bright ($B = +1.5$ T) and finally at $B = +2.0$ T all Co islands appear bright again. The same behavior is observed when the magnetic field sweep is reversed. From previous studies it is known that the Co islands switch in magnetic fields between $B = \pm0.5$ and ±2.5 T depending on their size [10,12,58]. Thus we can conclude that the first contrast change at $B = +0.5$ T is due the magnetization reversal of the tip. Such a behavior of bulk Cr tips has been observed in previous studies and was explained by uncompensated Cr spins that are sensitive to the external magnetic field [58]. All bulk Cr tips used in this work showed similar behavior.
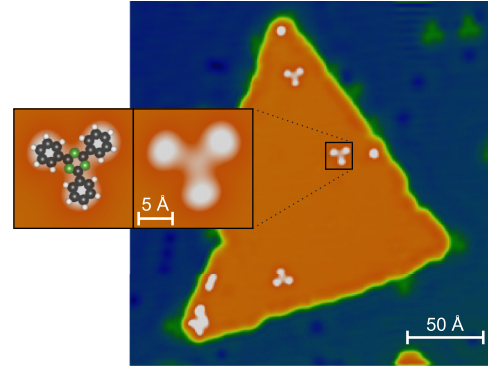

FIG. 5. Constant-current STM image of a Co island on Cu(111) after the deposition of TPT molecules ($V = -200$ mV and $I = 200$ pA). (Inset) Magnified STM image of a TPT molecule (right) overlaid with a graphical true-scale representation of the TPT molecule in the gas phase (left).

B. Adsorption of TPT on Co nanoislands

Having investigated the properties of bare Co islands, TPT molecules have been deposited on the same sample at low temperatures (see also Sec. II A) and then single TPT molecules on top of Co islands are imaged by STM [64–66]. Note that for the studies in this section a nonmagnetic tungsten tip has been used. Figure 5 shows an STM image of a Co island after the adsorption of the molecules. The TPT molecules can be clearly identified by their shape that resembles the structure of the molecule in the gas phase. This is emphasized by the overlaid graphical true-scale representation of the TPT molecule in the inset of Fig. 5. Fragments of the molecules are barely found, which indicates that most of the molecules stay intact after adsorption on the Co islands. Only at the edges of the Co islands impurities are observed, which are assumed to be fragments of the TPT molecule, since their shapes and sizes coincide with the phenyl rings of the intact molecules.

An analysis of many adsorbed TPT molecules reveals two preferred adsorption orientations on the Co islands (also recognizable in Fig. 5), which is reasonable if we consider the symmetries of the surface atomic lattice of the Co island and the TPT molecule. Due to the sixfold rotational symmetry of the uppermost Co layer we should expect six different adsorption geometries at first glance, but since the TPT molecule has a threefold symmetry, the six adsorption geometries are threefold degenerate, thus leading to two different adsorption orientations.

To determine the exact adsorption position of the TPT molecules on the Co islands, we have recorded STM images with atomic resolution. Since it is difficult to resolve the atomic structure of the Co islands with a bare metal tip in the presence of adsorbed TPT molecules without causing too much interaction, we have made use of a functionalized tip. From other works, it is known that functionalized tips can show unmatched spatial resolution [67–73]. Thus we have picked up an (occasionally adsorbed) CO molecule from the Cu(111) surface and imaged a TPT molecule and the underlying Co island with atomic resolution by approaching the functionalized tip to the surface [Figs. 6(a) and 6(b)]. Interestingly, we found that by coming closer to the surface the
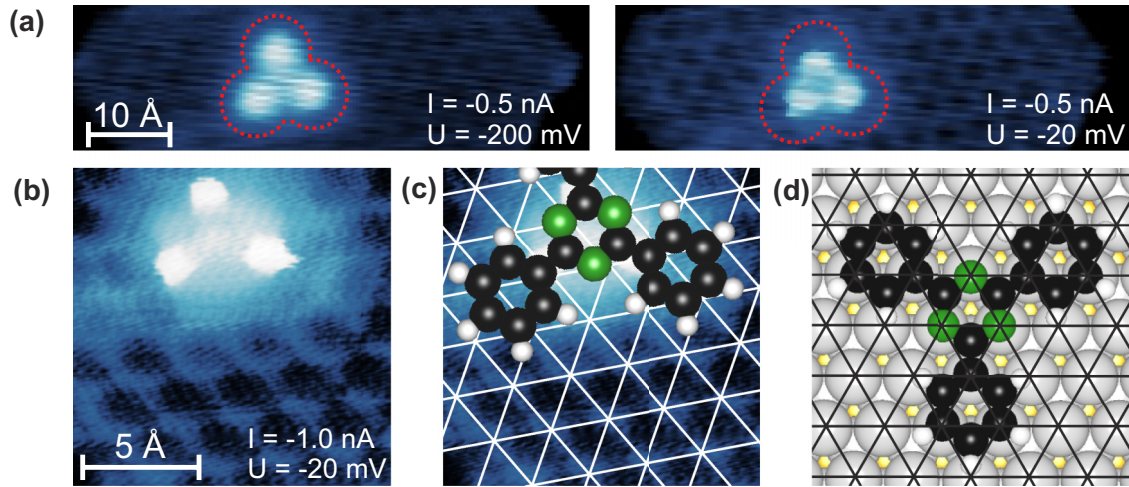
FIG. 6. (a) Constant-current STM images of a TPT molecule adsorbed on a fcc (unfaulted) Co island grown on Cu(111) for different tip-sample distances obtained with a CO functionalized tip. Already for small currents the atomic structure of the Co island is somewhat visible (left). For a smaller bias voltage (right), i.e., for a smaller tip-sample distance, the TPT molecule appears smaller compared to the left panel as indicated by the dotted red contours. (b) As panel (a), but for even smaller tip-sample distance. The real size of the TPT molecule is actually given by the blurred blue cloud. The atomic lattice of Co(111) is clearly visible. (c) STM image of panel b overlaid with the atomic structure of the Co island and the gas-phase structure of the TPT molecule. (d) Calculated adsorption geometry of TPT on 2Co/5Cu (see text).

TPT molecule appears much smaller than in reality [74]. This can be clearly seen in Fig. 6(a), which shows the same area for two different tip-sample distances. With decreasing tip-sample distance this effect becomes even more pronounced and the real size of the molecule is actually given by the blurred cloud that surrounds the bright center of the molecule. In Fig. 6(b), the atomic structure of the Co(111) surface is clearly seen. Note that the TPT molecule seems to be even smaller than in Fig. 6(a). The real size is again given by the blurred cloud. By overlaying the atomic lattice of the Co island and the gas-phase structure of the TPT molecule we can precisely identify the adsorption position of TPT [Fig. 6(c)]: the nitrogen atoms of the triazine ring adsorb on top of the Co atoms, leading to a symmetric adsorption geometry for all phenyl rings and thus to two distinguishable orientations on the Co islands. Note that the adsorption geometry was only experimentally determined for a TPT molecule adsorbed on an fcc (unfaulted) Co island. Nevertheless, we can assume that this adsorption site remains also valid for hcp (faulted) Co islands, since all types of islands, i.e., with different stackings, exhibit the same symmetry and electronic properties at the surface.

Our finding is also confirmed by the DFT calculations, as we find the highest binding energy (3.55 eV) for the experimentally observed adsorption geometry. As seen from Fig. 6(d), the calculated adsorption geometry is in excellent agreement with the experimental one. For reasons of simplicity, the DFT calculations have been only carried out for an fcc type stacking of the Co.

C. Electronic properties of TPT on Co islands

An important prerequisite for the formation of a hybrid molecular magnet is the hybridization with the ferromagnetic building block, i.e., in our case with the Co island. Thus we have to investigate the electronic properties of the adsorbed

TPT molecules in order to check if this precondition is fulfilled. For this purpose, we have measured differential conductance spectra at different locations on the molecule, namely, on the triazine and phenyl rings. Note that for the studies in this section a nonmagnetic tungsten tip has been used. Figure 7 shows typical dI/dV spectra, which reveal the main electronic features that we have observed during our measurements on different TPT molecules and also for different tips. Besides minor differences, all spectra show the same features, namely three peaks located at approximately -340, $+170$, and $+600$ mV. Note that the peak at -340 mV is located in the same energy region as the d-like surface state of the Co [compare with Fig. 3(a)]. This, and also the fact that only broad features are observed, leads to the conclusion that the molecule is strongly hybridized with the Co island, thus fulfilling the basic requirement for a hybrid molecular magnet.
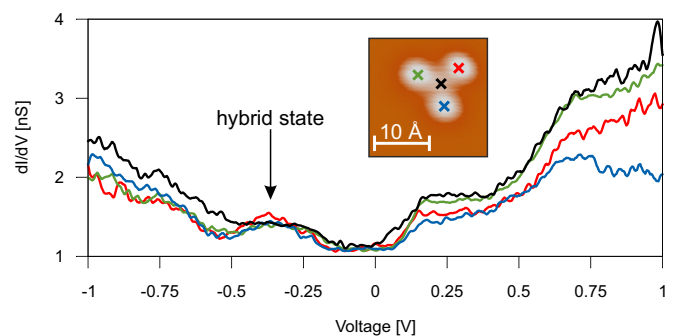

FIG. 7. Differential conductance dI/dV spectra acquired on the different aromatic rings of the TPT molecule. For the measurement, a nonmagnetic tungsten tip has been used. The inset shows the STM image of the corresponding TPT molecule with the marked spectroscopy locations ($V = -200$ mV and $I = 200$ pA).

The slightly different electronic properties of the phenyl rings at higher energies, mainly above +700 mV, seem surprising at first glance, since the adsorption site and geometry are identical for all phenyl rings as revealed by our analysis of the adsorption geometry in section III B. Significant intramolecular variations of the electronic and magnetic properties among the aromatic rings have recently been observed for TPT molecules adsorbed on 2-ML Fe on W(110) [27]. In this case, the combination of the threefold symmetric TPT molecule and the twofold symmetric substrate lattice leads to a highly asymmetric and chiral adsorption geometry with different bonding and hybridization conditions for the three peripheral phenyl groups in each TPT molecule. In the present case, the threefold symmetry is not broken by the adsorption process, but if we take into account the presence of the standing electron waves on the Co nanoislands due to the confinement of the *sp* electrons, then the most probable explanation for the differences among the phenyl groups is that they are related to the spatial modulation of the *sp* surface state. This seems reasonable, since the periodicity of standing waves at this energy is of the order of 10 Å [see Fig. 3(b)] and thus comparable with the size of the molecule. The small intramolecular variations among the peripheral phenyl groups emphasize why it is important to carry out the spin-polarized measurements for different spin configurations between tip and sample on the same molecule.

For simplicity, we will call the state located at −340 mV in the following *hybrid state*, since we are going to show in Sec. III D that this state is not just the *d*-like surface state measured through the TPT molecule, but a manifestation of a new hybrid electronic structure due to the hybridization with the Co island and that this state exhibits the strongest spin-dependent effect. Note that we do not observe major differences between TPT molecules adsorbed on fcc (unfaulted) or hcp (faulted) Co islands, respectively. The only difference is that the position of the hybrid state shifted slightly (<50 mV), which correlates with the shift of the *d*-like surface state of Co reported in Ref. [60].

D. Magnetic properties of the hybrid system

Having investigated the electronic properties of the TPT molecules on the Co islands, we finally turn to their magnetic properties. For this purpose, we use a bulk Cr tip prepared according to the description in Sec. II B. The tip showed the same behavior as the one in Sec. III A. This means that the magnetization direction of the Cr tip can be reversed by applying an external magnetic field of $B = \pm0.5$ T. We have used this feature to measure spin-resolved dI/dV maps and differential conductance spectra of the TPT molecules for parallel (P) and antiparallel (AP) alignments of the tip and sample magnetization directions.

However, before we turn to the spin-resolved dI/dV maps and dI/dV spectra of TPT, it is important to define the parallel and antiparallel spin configurations. To this end, we applied an external magnetic field of $B = +1.75$ T in order to align the magnetization of the Co islands with the external field. The switching of the Co islands was confirmed by taking a dI/dV map at −500 mV (analogous to the procedure in Sec. III A). Then we switched the magnetization of the tip by sweeping
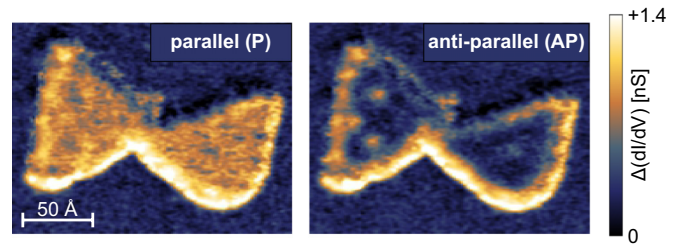

FIG. 8. dI/dV maps of Co islands on Cu(111) with adsorbed TPT molecules for parallel and antiparallel magnetization orientations between tip and Co island measured with a bulk Cr tip ($V = -500$ mV and $I = 1.5$ nA). The switching between the two states is caused by the magnetization reversal of the tip magnetization in the external magnetic field B.

the external magnetic field to $B = -0.5$ T and measured again a dI/dV map at −500 mV. We define the state in which we observed a high differential conductance signal as parallel and accordingly the state with low conductance as antiparallel. The dI/dV maps of the Co islands (with the adsorbed TPT molecules) are shown in Fig. 8 and correspond to the parallel and antiparallel states, respectively. Before measuring spin-resolved dI/dV maps and dI/dV spectra of TPT, we always confirmed the actual state (P or AP) by dI/dV maps of the particular Co islands.

To determine the spin polarization of the TPT molecules, we calculated the spin asymmetry

$$A = \frac{(dI/dV)_{\mathrm{AP}} - (dI/dV)_{\mathrm{P}}}{(dI/dV)_{\mathrm{AP}} + (dI/dV)_{\mathrm{P}}}, \qquad (1)$$

where $(dI/dV)_{\mathrm{AP}}$ and $(dI/dV)_{\mathrm{P}}$ are the differential conductance signals in AP and P configuration, respectively. The spin asymmetry A is related to the spin polarization P_{S} of the sample at the position of the tip, and to the spin polarization P_{T} of the tip via

$$A = -P_{\mathrm{S}}P_{\mathrm{T}}. \qquad (2)$$

Since the spin polarization of the tip, P_{T}, does not vary spatially above the sample for a fixed bias voltage, we can assume that variations in the spatially resolved spin asymmetry A are linked to the spin polarization of the sample, that is, $A \propto P_{\mathrm{S}}$.

Figure 9 exemplarily shows the spin-resolved dI/dV spectra of the different aromatic rings of one TPT molecule. As seen, the strongest spin-dependent effect occurs for the hybrid state. All other states show hardly any spin polarization. Currently, it is not known if the STM tip was not spin sensitive in these energy ranges, or if the TPT molecules are not spin-polarized in these energy ranges. Note that the peak at ≈-80 mV was not detected in the spin-averaged measurements before and thus is most probably a tip state. This is emphasized by the fact that also in the differential conductance spectra on the bare Co islands (gray curve) a peak at this energy (≈-80 mV) is recognizable. Having a tip state in the gaplike structure of the TPT/Co spectrum (see also section III C) is unfortunate but reveals how difficult it is to prepare a STM tip with good electronic properties (i.e., flat DOS near the Fermi energy), spatial resolution (e.g., no double tips) and with magnetic sensitivity. Interestingly, the hybrid
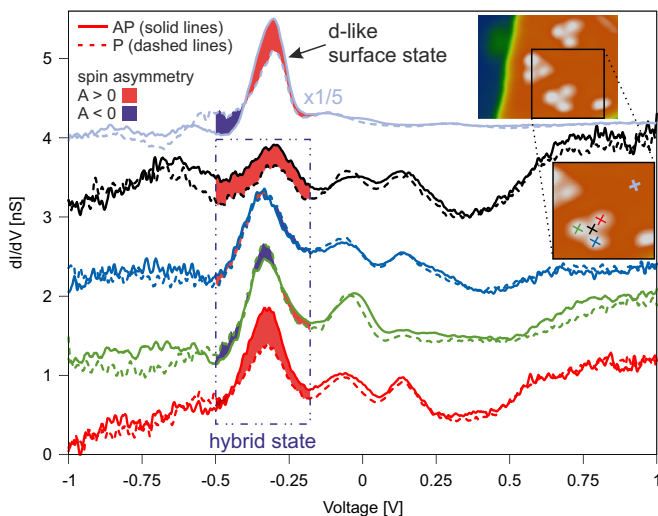
FIG. 9. Spin-resolved differential conductance dI/dV spectra acquired on the different aromatic rings of the TPT molecule (red, green, blue, black) and for comparison far from the molecule (gray) for parallel (P) and antiparallel (AP) configuration between tip and Co island. The color of the filled areas between the dI/dV spectra for AP and P configuration indicates the sign of the spin asymmetry A. For the measurement a bulk Cr tip has been used. The different spectroscopy locations on the TPT molecule are marked in the STM image in the inset ($V = -200$ mV and $I = 200$ pA). Spectra are vertically shifted for clarity and the gray spectrum measured on bare Co is divided by 5.

state exhibits different spin polarizations on the different aromatic rings of the TPT molecule. The spin polarization of the hybrid state is inverted (green curve) or has the same sign (red curve) in comparison to the spin polarization of the d-like surface state (gray curve), or shows no spin polarization (blue curve). The spin asymmetry of the hybrid state at different locations on the TPT molecule and on the uncovered Co island extracted from the data in Fig. 9 are listed in Table I.

Before discussing the possible origin of the varying spin polarizations on the different aromatic rings of a TPT molecule we note that the spin-resolved spectra of the Co island (gray curves) show the typical behavior known from literature [10,58]. The varying spin polarizations on the aromatic rings of the TPT molecules cannot be explained by a different hybridization of the aromatic rings, because TPT adsorbs highly symmetric on the Co islands (see Sec. III B). Hence the three phenyl rings have the same adsorption sites and should hybridize equally with the Co island. Thus the spin-dependent properties should be also equal, but, as seen in Fig. 9, they

TABLE I. Spin asymmetry A of the hybrid state around -310 mV derived from the spectra in Fig. 9. The error margins are estimated from the noise of each spectrum.

Spin asymmetry A (%)				
TPT red	TPT green	TPT blue	TPT black	Co gray
13.0 ± 2.9	-5.6 ± 2.8	1.5 ± 2.2	10.1 ± 3.7	16.0 ± 0.8

exhibit different spin polarizations. This variation in the spin polarization also demonstrates that the hybrid state is not just the d-like surface state of Co which shows through the molecules but a new state formed due to the hybridization of the molecular states and the d-like surface state, because the spin polarization of the latter one does not change its sign within the Co islands.

In order to gain a better insight into the spatial variations of the spin polarization of the hybrid state of TPT we measured spatially resolved dI/dV maps in AP and P configurations at the energy of the hybrid state of TPT, that is, $V = -310$ mV in this particular case (see Fig. 9). Figure 10(a) shows a constant-current STM image of TPT molecules adsorbed on a Co island, and Figs. 10(b) and 10(c) show the dI/dV maps in AP and P configurations, respectively. Note that this Co island is the same as in the inset of Fig. 9 and that the different contrast in Figs. 8 and 10 stems from the strongly different range of the displayed dI/dV values. The resultant spatially resolved map of the spin asymmetry according to Eq. (1) is shown in Fig. 10(d). To make the analysis easier, the map of the spin asymmetry has been smoothed by removing the high frequency noise using a Gaussian filter [Fig. 10(e)], and in addition graphical representations of the TPT molecules have been overlaid in Fig. 10(f). The spin asymmetry maps are shown using the discrete color scale shown on the right-hand side.

As seen in Figs. 10(e) and 10(f), the spin asymmetry A, and consequently the spin polarization P_S of the sample, shows a strong spatial modulation within the Co island. The strongest effects occur around the TPT molecules, namely the spin asymmetry A exhibits positive and negative values. This change occurs on a length scale of approximately 13 Å as indicated in Fig. 10(f). Such a change in the sign of the spin asymmetry is not observed in areas, where no molecules are adsorbed—there the spin polarization only shows positive values, but also varies on a length scale of $\approx$13 Å from minimum to maximum [see Fig. 10(f)].

IV. DISCUSSION

In order to exclude that the observed variations in the spin polarization stem from our measuring inaccuracy, we estimated the uncertainty of the measured spin polarization. In our STM setup, the stability of the tunneling junction is roughly ± 1 pm. According to Ref. [75], the relation between spin-dependent height differences (Δz) and the spin polarization is given by

$$P_S P_T = \frac{\exp(A\sqrt{\phi}\Delta z) - 1}{\exp(A\sqrt{\phi}\Delta z) + 1}. \tag{3}$$

For a typical work function $\phi \approx 4$ eV, the constant $A \approx 1$ eV$^{-1/2}$ Å^{-1}, and $\Delta z = 2$ pm this leads to $P_S P_T \approx 2\%$. Hence the uncertainty of the measured spin polarization in our setup is about 2%. As seen from Fig. 10(d), the observed changes in the spin polarization exceed this value. Thus both the observed spatial modulation of the spin polarization on the uncovered Co island and the intramolecular variations on the different aromatic rings of the TPT molecules are real effects. Furthermore, we have observed and confirmed similar
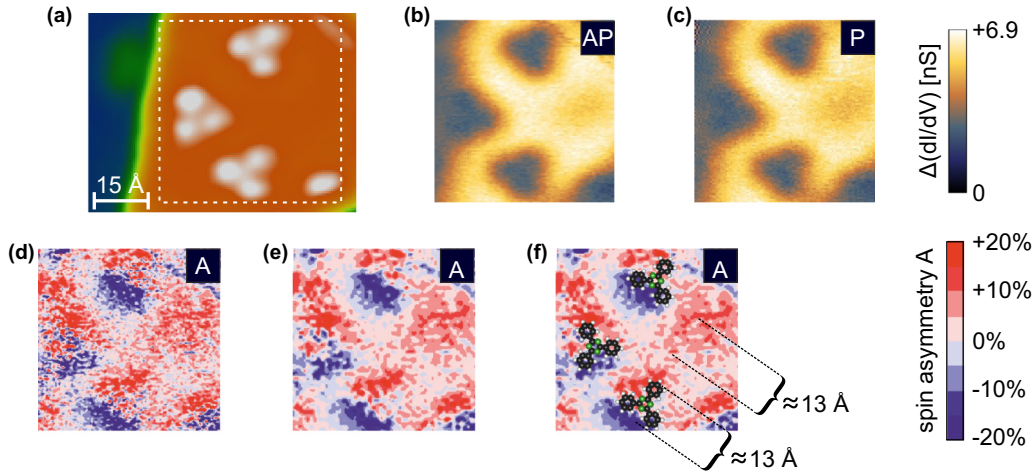
FIG. 10. (a) Constant-current STM image of a Co island with adsorbed TPT molecules ($V = -200$ mV and $I = 200$ pA). Note that the Co island is the same as in Fig. 9. (b) dI/dV map of the Co island with adsorbed TPT molecules at the energy of the hybrid state for antiparallel magnetization directions between tip and sample measured with a bulk Cr tip ($V = -310$ mV and $I = 1.5$ nA). Image section corresponds to the area indicated in (a). (c) As (b), but for the parallel state. (d) Spin asymmetry map calculated from the dI/dV maps in (b) and (c) according to Eq. (1). (e) and (f) The spin asymmetry map from (d) after applying a Gaussian filter to remove the noise. (f) For the purpose of illustration, the graphical representation of the TPT molecule has been overlaid to the map in (e). The positions of the TPT molecules have been extracted from the simultaneously recorded constant-current image.

variations of the spin polarization among the aromatic rings of a TPT molecule on four different Co islands and in total for seven different TPT molecules, while using two different Cr bulk tips. Finally, we point out that the spin asymmetry values at the five locations in Fig. 10(f), where the spectra in Fig. 9 were taken, are in good correspondence with the spin asymmetry values in Table I.

As mentioned in Sec. III A, it has been shown in previous works that Co nanoislands exhibit varying spin polarizations due to the difference between the spatially modulated DOS of the sp surface state and the nonmodulated d-like surface state [33]. Depending on the energy, the periodicity of the spatial modulation of the spin polarization is in the order of ≈ 10–30 Å [33,59]. The changes in the spin polarization in Fig. 10(f) also occur on a length scale of ≈ 13 Å (periodicity of ≈ 26 Å), as mentioned above, and thus are most likely linked to the spin-dependent interference pattern of the Co nanoisland. The spin modulation pattern depends on the island edges and other scattering centers (e.g., defects, adsorbates) and, thus, in general does not exhibit a threefold symmetry. Therefore the influence of spin polarization pattern due to the interference of the Co(111) surface state is an obvious explanation for the observed broken threefold symmetry of the spin polarization within a single chemisorbed TPT molecule, which according to our STM images (Fig. 5) and DFT calculations (Fig. 2) forms a structurally threefold symmetric hybrid molecule-surface system. Note that the sp surface state of the clean Co(111) starts at approximately -0.17 V below the Fermi level [33,59] as mentioned in Sec. III A and thus is not expected to be present in the energy range of the hybrid state. Nevertheless, a quantum inference pattern can be clearly recognized in Fig. 10. This can be explained by assuming that the adsorption of a sufficient number of TPT molecules on the Co islands leads to a shift of the sp surface state to lower energies. Such a behavior has been observed for other systems, where the surface state shifts linearly with increasing adsorbate coverage. For example, such

a shift to lower energies is reported for the surface states of Pd(111) and Cu(111) due to the adsorption of H and O, respectively [76,77]. Shifts to higher energies have also been reported, e.g., for metallocenes on Cu(111) [78]. Furthermore, we conclude that the inversion of the spin polarization must be related to the presence of the TPT molecules and cannot be explained solely by the properties of the Co island, since the inversion of the spin polarization only occurs in the vicinity of the TPT molecules.

Hence, to explain the possible origin of the strongly varying spin polarizations around the TPT molecules, we propose a model where the molecules act as additional scattering centers for the electrons of the sp surface state, and thus modulate the intensity of the spin-dependent quantum interference pattern of the Co nanoislands similar to the effect reported in Ref. [79] for the rim of the islands. Since the wave function of the sp surface state cannot vanish abruptly at the edges of the TPT molecule, but rather extends into the molecules, a superposition of the spin polarization of TPT and of the modulated sp surface state is detected above the TPT molecules in the spin-resolved STM measurements. In Fig. 11(a), the different states, i.e., the nonmodulated d-like surface state, the hybrid state and the spatially modulated sp surface state, which contribute to the spin-resolved signal, are schematically illustrated as a function of the position on the Co island. The observed magnitudes of the spin asymmetries [see Fig. 11(b)] can be explained within this model under the assumption that the additional scattering processes lead to an enhancement of spin polarization of the sp surface state at the boundaries of the molecules and that the spin polarization of the hybrid state is inverted in comparison to the d-like surface state of the Co island. An inversion of the spin polarization of the hybrid state in comparison to the d-like surface state is reasonable, since we deduced in Sec. III C that the TPT molecules must be strongly hybridized with the Co islands, and a strong hybridization results in a inversion of the spin polarization in agreement with previous
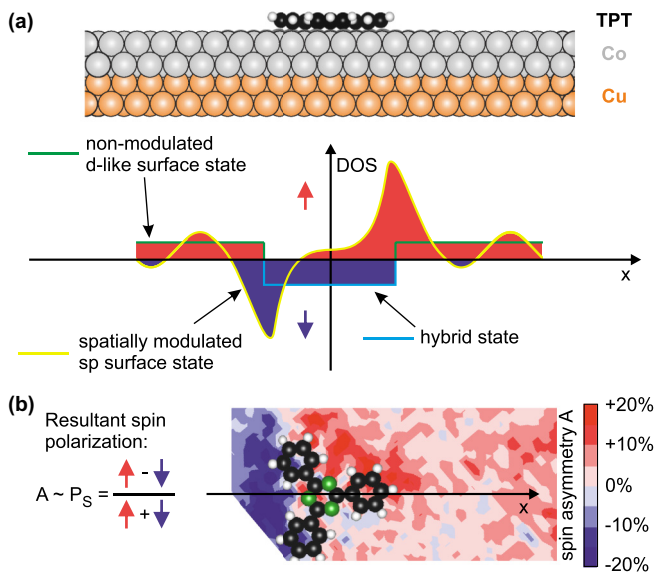
FIG. 11. (a) Illustration of the spin-resolved DOS of the nonmodulated d-like surface state, the hybrid state and the spatially modulated sp surface state depending on the position on the Co island. (b) The DOS illustrated in panel a results in a spin polarization pattern as observed in the experiment. The shown spin asymmetry map is an image section of Fig. 10(e).

combined STM and DFT studies [27,31,32] and model calculations [20].

V. CONCLUSION

In this work, we have analyzed systematically the formation of single molecular spin hybrids on Co islands on Cu(111) by means of spin-polarized scanning tunneling microscopy and spectroscopy (SP-STM/STS). The spin-sensitive measurements revealed that the spin polarization varies among the different aromatic rings of the TPT molecule, although the

molecules exhibit a highly symmetric adsorption geometry as revealed by atomically resolved STM images and confirmed by *ab initio* calculations that yield the highest binding energy for the experimentally ascertained adsorption site. Hence the varying degree of spin polarization on the different aromatic rings cannot stem from a different hybridization of the aromatic rings with the ferromagnetic substrate as recently observed for TPT on Fe/W(110) [27]. Given that the spatially resolved spin asymmetry maps also showed a modulation of the spin polarization on the uncovered parts of the Co islands, we propose to link the appearance of the intramolecular variations of the spin polarization to a superposition of the spin polarization of the TPT molecule and the spatially modulated spin-polarized sp surface state of the Co(111) surface. This emphasizes the importance to consider effects due to quantum confinement when tailoring molecular spin hybrids on magnetic nanostructures.

Our results demonstrate the formation of a single molecular spin hybrid, i.e., a molecule that is spin-dependently hybridized with a ferromagnetic surface, using a polyaromatic molecule and that the aromatic rings within the molecule can exhibit different spin polarizations. In further studies it will be interesting to explore to what extent the spin properties of hybrid molecular magnets can be modified by spin-dependent quantum interference patterns and to analyze the effect of the magnetic field on the hybrid molecular magnet in more detail to find out if the aromatic rings react differently on the magnetic field, e.g., if they switch at different magnetic fields.

[1] L. Bogani and W. Wernsdorfer, Molecular spintronics using single-molecule magnets, Nat. Mater. **7**, 179 (2008).

[2] T. Dietl, D. D. Awschalom, M. Kaminska, and H. Ohno, *Spintronics* (Academic Press Inc., London, 2009), Vol. 82.

[3] S. A. Wolf, D. D. Awschalom, R. A. Buhrman, J. M. Daughton, S. von Molnar, M. L. Roukes, A. Y. Chtchelkanova, and D. M. Treger, Spintronics: A spin-based electronics vision for the future, Science **294**, 1488 (2001).

[4] A. R. Rocha, V. M. Garcia-Suarez, S. W. Bailey, C. J. Lambert, J. Ferrer, and S. Sanvito, Towards molecular spintronics, Nat. Mater. **4**, 335 (2005).

[5] M. N. Leuenberger and D. Loss, Quantum computing in molecular magnets, Nature (London) **410**, 789 (2001).

[6] T. D. Ladd, F. Jelezko, R. Laflamme, Y. Nakamura, C. Monroe, and J. L. O'Brien, Quantum computers, Nature (London) **464**, 45 (2010).

[7] D. Loss and D. P. DiVincenzo, Quantum computation with quantum dots, Phys. Rev. A **57**, 120 (1998).

[8] C. H. Bennett and D. P. DiVincenzo, Quantum information and computation, Nature (London) **404**, 247 (2000).

[9] D. P. DiVincenzo, Quantum computation, Science **270**, 255 (1995).

[10] O. Pietzsch, A. Kubetzka, M. Bode, and R. Wiesendanger, Spin-Polarized Scanning Tunneling Spectroscopy of Nanoscale Cobalt Islands on Cu (111), Phys. Rev. Lett. **92**, 057202 (2004).

[11] S. Wedekind, G. Rodary, J. Borme, S. Ouazi, Y. Nahas, M. Corbetta, H. Oka, D. Sander, and J. Kirschner, Switching fields of individual Co nanoislands, IEEE Trans. Magn. **47**, 3351 (2011).

[12] S. Ouazi, S. Wedekind, G. Rodary, H. Oka, D. Sander, and J. Kirschner, Magnetization Reversal of Individual Co Nanoislands, Phys. Rev. Lett. **108**, 107206 (2012).

[13] G. Christou, D. Gatteschi, D. N. Hendrickson, and R. Sessoli, Single-molecule magnets, MRS Bull. **25**, 66 (2000).

[14] A. Scheybal, T. Ramsvik, R. Bertschinger, M. Putero, F. Nolting, and T. Jung, Induced magnetic ordering in a molecular monolayer, Chem. Phys. Lett. **411**, 214 (2005).

[15] H. Wende, M. Bernien, J. Luo, C. Sorg, N. Ponpandian, J. Kurde, J. Miguel, M. Piantek, X. Xu, P. Eckhold *et al.*, Substrate-induced magnetic ordering and switching of iron porphyrin molecules, Nat. Mater. **6**, 516 (2007).

[16] M. Bernien, J. Miguel, C. Weis, M. E. Ali, J. Kurde, B. Krumme, P. M. Panchmatia, B. Sanyal, M. Piantek, and P. Srivastava *et al.*, Tailoring the Nature of Magnetic Coupling of Fe-Porphyrin Molecules to Ferromagnetic Substrates, Phys. Rev. Lett. **102**, 047202 (2009).

[17] E. Annese, J. Fujii, I. Vobornik, G. Panaccione, and G. Rossi, Control of the magnetism of cobalt phthalocyanine by a ferromagnetic substrate, Phys. Rev. B **84**, 174443 (2011).

[18] M. Gruber, F. Ibrahim, S. Boukari, H. Isshiki, L. Joly, M. Peter, M. Studniarek, V. Da Costa, H. Jabbar, V. Davesne *et al.*, Exchange bias and room-temperature magnetic order in molecular layers, Nat. Mater. **14**, 981 (2015).

[19] M. Callsen, V. Caciuc, N. Kiselev, N. Atodiresei, and S. Blügel, Magnetic Hardening Induced by Nonmagnetic Organic Molecules, Phys. Rev. Lett. **111**, 106805 (2013).

[20] M. Galbiati, S. Tatay, C. Barraud, A. V. Dediu, F. Petroff, R. Mattana, and P. Seneor, Spinterface: Crafting spintronics at the molecular scale, MRS Bull. **39**, 602 (2014).

[21] K. V. Raman, A. M. Kamerbeek, A. Mukherjee, N. Atodiresei, T. K. Sen, P. Lazić, V. Caciuc, R. Michel, D. Stalke, S. K. Mandal *et al.*, Interface-engineered templates for molecular spin memory devices, Nature (London) **493**, 509 (2013).

[22] K. Bairagi, A. Bellec, V. Repain, C. Chacon, Y. Girard, Y. Garreau, J. Lagoute, S. Rousset, R. Breitwieser, Y.-C. Hu *et al.*, Tuning the Magnetic Anisotropy at a Molecule-Metal Interface, Phys. Rev. Lett. **114**, 247203 (2015).

[23] R. Friedrich, V. Caciuc, N. S. Kiselev, N. Atodiresei, and S. Blügel, Chemically functionalized magnetic exchange interactions of hybrid organic-ferromagnetic metal interfaces, Phys. Rev. B **91**, 115432 (2015).

[24] R. Friedrich, V. Caciuc, N. Atodiresei, and S. Blügel, Molecular induced skyhook effect for magnetic interlayer softening, Phys. Rev. B **92**, 195407 (2015).

[25] T. Miyamachi, M. Gruber, V. Davesne, M. Bowen, S. Boukari, L. Joly, F. Scheurer, G. Rogez, T. K. Yamada, P. Ohresser *et al.*, Robust spin crossover and memristance across a single molecule, Nat. Commun. **3**, 938 (2012).

[26] D. E. Bürgler, V. Heß, T. Esat, S. Fahrendorf, F. Matthes, C. M. Schneider, C. Besson, K. Y. Monakhov, P. Kögerler, A. Ghisolfi *et al.*, Spin-Hybrids: A Single-Molecule Approach to Spintronics, e-J. Surf. Sci. Nanotechnol. **14**, 17 (2016).

[27] V. Heß, R. Friedrich, F. Matthes, V. Caciuc, N. Atodiresei, D. E. Bürgler, S. Blügel, and C. M. Schneider, Magnetic subunits within a single molecule-surface hybrid (unpublished).

[28] C. Barraud, P. Seneor, R. Mattana, S. Fusil, K. Bouzehouane, C. Deranlot, P. Graziosi, L. Hueso, I. Bergenti, V. Dediu *et al.*, Unravelling the role of the interface for spin injection into organic semiconductors, Nat. Phys. **6**, 615 (2010).

[29] S. Steil, N. Großmann, M. Laux, A. Ruffing, D. Steil, M. Wiesenmayer, S. Mathias, O. L. Monti, M. Cinchetti, and M. Aeschlimann, Spin-dependent trapping of electrons at spinterfaces, Nat. Phys. **9**, 242 (2013).

[30] F. Djeghloul, M. Gruber, E. Urbain, D. Xenioti, L. Joly, S. Boukari, J. Arabski, H. Bulou, F. Scheurer, F. Bertran *et al.*, High spin polarization at ferromagnetic metal-organic

interfaces: A generic property, J. Phys. Chem. Lett. **7**, 2310 (2016).

[31] J. Brede, N. Atodiresei, S. Kuck, P. Lazić, V. Caciuc, Y. Morikawa, G. Hoffmann, S. Blügel, and R. Wiesendanger, Spin- and Energy-Dependent Tunneling Through a Single Molecule with Intramolecular Spatial Resolution, Phys. Rev. Lett. **105**, 047204 (2010).

[32] N. Atodiresei, J. Brede, P. Lazić, V. Caciuc, G. Hoffmann, R. Wiesendanger, and S. Blügel, Design of the Local Spin Polarization at the Organic-Ferromagnetic Interface, Phys. Rev. Lett. **105**, 066601 (2010).

[33] H. Oka, P. A. Ignatiev, S. Wedekind, G. Rodary, L. Niebergall, V. S. Stepanyuk, D. Sander, and J. Kirschner, Spin-Dependent Quantum Interference within a Single Magnetic Nanostructure, Science **327**, 843 (2010).

[34] J. de la Figuera, J. E. Prieto, C. Ocal, and R. Miranda, Scanning-tunneling-microscopy study of the growth of cobalt on Cu (111), Phys. Rev. B **47**, 13043(R) (1993).

[35] N. N. Negulyaev, V. S. Stepanyuk, P. Bruno, L. Diekhöner, P. Wahl, and K. Kern, Bilayer growth of nanoscale Co islands on Cu (111), Phys. Rev. B **77**, 125437 (2008).

[36] A. Rabe, N. Memmel, A. Steltenpohl, and T. Fauster, Room-Temperature Instability of Co/Cu (111), Phys. Rev. Lett. **73**, 2728 (1994).

[37] M. Cavallini and F. Biscarini, Electrochemically etched nickel tips for spin polarized scanning tunneling microscopy, Rev. Sci. Instrum. **71**, 4457 (2000).

[38] R. Koltun, M. Herrmann, G. Güntherodt, and V. A. M. Brabers, Enhanced atomic-scale contrast on Fe_3O_4 (100) observed with an Fe STM tip, Appl. Phys. A **73**, 49 (2001).

[39] C. Albonetti, I. Bergenti, M. Cavallini, V. Dediu, M. Massi, J.-F. Moulin, and F. Biscarini, Electrochemical preparation of cobalt tips for scanning tunneling microscopy, Rev. Sci. Instrum. **73**, 4254 (2002).

[40] A. L. Bassi, C. S. Casari, D. Cattaneo, F. Donati, S. Foglio, M. Passoni, C. E. Bottani, P. Biagioni, A. Brambilla, M. Finazzi *et al.*, Bulk Cr tips for scanning tunneling microscopy and spin-polarized scanning tunneling microscopy, Appl. Phys. Lett. **91**, 173120 (2007).

[41] A. Schlenhoff, S. Krause, G. Herzog, and R. Wiesendanger, Bulk Cr tips with full spatial magnetic sensitivity for spin-polarized scanning tunneling microscopy, Appl. Phys. Lett. **97**, 083104 (2010).

[42] R. Wiesendanger, D. Bürgler, G. Tarrach, T. Schaub, U. Hartmann, H.-J. Güntherodt, I. V. Shvets, and J. M. D. Coey, Recent advances in scanning tunneling microscopy involving magnetic probes and samples, Appl. Phys. A **53**, 349 (1991).

[43] M. Bode, Spin-polarized scanning tunneling microscopy, Rep. Prog. Phys. **66**, 523 (2003).

[44] A. Kubetzka, M. Bode, O. Pietzsch, and R. Wiesendanger, Spin-Polarized Scanning Tunneling Microscopy with Antiferromagnetic Probe Tips, Phys. Rev. Lett. **88**, 057201 (2002).

[45] G. Rodary, S. Wedekind, H. Oka, D. Sander, and J. Kirschner, Characterization of tips for spin-polarized scanning tunneling microscopy, Appl. Phys. Lett. **95**, 152513 (2009).

[46] R. Wiesendanger, Spin mapping at the nanoscale and atomic scale, Rev. Mod. Phys. **81**, 1495 (2009).

[47] Since bulk Cr has no net magnetization the term "tip magnetization" refers here to the magnetic moment of the frontmost

atom or of the uncompensated spins at the Cr tip apex that can be reversed by an external magnetic field.

[48] P. Hohenberg and W. Kohn, Inhomogeneous electron gas, Phys. Rev. **136**, B864 (1964).

[49] W. Kohn and L. Sham, Self-consistent equations including exchange and correlation effects, Phys. Rev. **140**, A1133 (1965).

[50] G. Kresse and J. Hafner, *Ab initio* molecular-dynamics simulation of the liquid-metal–amorphous-semiconductor transition in germanium, Phys. Rev. B **49**, 14251 (1994).

[51] G. Kresse and J. Furthmüller, Efficient iterative schemes for ab initio total-energy calculations using a plane-wave basis set, Phys. Rev. B **54**, 11169 (1996).

[52] G. Kresse and J. Furthmüller, Efficiency of *ab-initio* total energy calculations for metals and semiconductors using a plane-wave basis set, Comput. Mater. Sci. **6**, 15 (1996).

[53] P. E. Blöchl, Projector augmented-wave method, Phys. Rev. B **50**, 17953 (1994).

[54] J. P. Perdew, K. Burke, and M. Ernzerhof, Generalized Gradient Approximation Made Simple, Phys. Rev. Lett. **77**, 3865 (1996).

[55] N. Atodiresei, V. Caciuc, J.-H. Franke, and S. Blügel, Role of the van der Waals interactions on the bonding mechanism of pyridine on Cu(110) and Ag(110) surface: First-principles study, Phys. Rev. B **78**, 045411 (2008).

[56] The adsorption energy is defined as $E_{\text{ads}} = -(E_{\text{sys}} - (E_{\text{surf}} + E_{\text{molec}}))$, where E_{sys} is the total energy of the molecule–surface system, E_{surf} represents the total energy of the 2-ML Co/Cu(111) surface, and E_{molec} stands for the total energy of the isolated molecule.

[57] O. Pietzsch, S. Okatov, A. Kubetzka, M. Bode, S. Heinze, A. Lichtenstein, and R. Wiesendanger, Spin-Resolved Electronic Structure of Nanoscale Cobalt Islands on Cu (111), Phys. Rev. Lett. **96**, 237203 (2006).

[58] G. Rodary, S. Wedekind, D. Sander, and J. Kirschner, Magnetic hysteresis loop of single Co nano-islands, Jpn. J. Appl. Phys. **47**, 9013 (2008).

[59] L. Diekhöner, M. A. Schneider, A. N. Baranov, V. S. Stepanyuk, P. Bruno, and K. Kern, Surface States of Cobalt Nanoislands on Cu (111), Phys. Rev. Lett. **90**, 236801 (2003).

[60] M. V. Rastei, B. Heinrich, L. Limot, P. A. Ignatiev, V. S. Stepanyuk, P. Bruno, and J. P. Bucher, Size-Dependent Surface States of Strained Cobalt Nanoislands on Cu (111), Phys. Rev. Lett. **99**, 246102 (2007).

[61] D. Sander, H. Oka, M. Corbetta, V. Stepanyuk, and J. Kirschner, New insights into nano-magnetism by spin-polarized scanning tunneling microscopy, J. Electron Spectrosc. Relat. Phenom. **189**, 206 (2013).

[62] J. Izquierdo, A. Vega, and L. C. Balbás, Magnetism of Co nanoparticles supported on the Cu (111) substrate: Size and environment dependence, Phys. Rev. B **55**, 445 (1997).

[63] L. Niebergall, V. S. Stepanyuk, J. Berakdar, and P. Bruno, Controlling the Spin Polarization of Nanostructures on Magnetic Substrates, Phys. Rev. Lett. **96**, 127204 (2006).

[64] C. Iacovita, M. V. Rastei, B. W. Heinrich, T. Brumme, J. Kortus, L. Limot, and J. P. Bucher, Visualizing the Spin of Individual Cobalt-Phthalocyanine Molecules, Phys. Rev. Lett. **101**, 116602 (2008).

[65] X. Fei, G. Wu, V. Lopez, G. Lu, H.-J. Gao, and L. Gao, Spin-dependent conductance in $Co/C_{60}/Co/Ni$ single-molecule junctions in the contact regime, J. Phys. Chem. C **119**, 11975 (2015).

[66] S. Gueddida, M. Gruber, T. Miyamachi, E. Beaurepaire, W. Wulfhekel, and M. Alouani, Exchange coupling of spin-crossover molecules to ferromagnetic Co islands, J. Phys. Chem. Lett. **7**, 900 (2016).

[67] R. Temirov, S. Soubatch, O. Neucheva, A. C. Lassise, and F. S. Tautz, A novel method achieving ultra-high geometrical resolution in scanning tunneling microscopy, New J. Phys. **10**, 053012 (2008).

[68] C. Weiss, C. Wagner, R. Temirov, and F. S. Tautz, Direct imaging of intermolecular bonds in scanning tunneling microscopy, J. Am. Chem. Soc. **132**, 11864 (2010).

[69] C. Weiss, C. Wagner, C. Kleimann, M. Rohlfing, F. S. Tautz, and R. Temirov, Imaging Pauli Repulsion in Scanning Tunneling Microscopy, Phys. Rev. Lett. **105**, 086103 (2010).

[70] G. Kichin, C. Weiss, C. Wagner, F. S. Tautz, and R. Temirov, Single molecule and single atom sensors for atomic resolution imaging of chemically complex surfaces, J. Am. Chem. Soc. **133**, 16847 (2011).

[71] P. Hapala, G. Kichin, C. Wagner, F. S. Tautz, R. Temirov, and P. Jelínek, Mechanism of high-resolution STM/AFM imaging with functionalized tips, Phys. Rev. B **90**, 085421 (2014).

[72] P. Hapala, R. Temirov, F. S. Tautz, and P. Jelínek, Origin of High-Resolution IETS-STM Images of Organic Molecules with Functionalized Tips, Phys. Rev. Lett. **113**, 226101 (2014).

[73] L. Gross, F. Mohn, N. Moll, P. Liljeroth, and G. Meyer, The chemical structure of a molecule resolved by atomic force microscopy, Science **325**, 1110 (2009).

[74] Note that this effect only occurred for the functionalized tip and is most probably related to the peculiarities of this imaging mode. Since the CO molecule is not stiff on the tip, but has some degrees of freedom to move without breaking the CO-tip bond, the most probable explanation is that the CO molecule bends at closer tip-surface distances due to the stronger interaction with the TPT molecule. This bending then results in a distortion of the image of the measured TPT molecule.

[75] R. Wiesendanger, H.-J. Güntherodt, G. Güntherodt, R. J. Gambino, and R. Ruf, Observation of Vacuum Tunneling of Spin-Polarized Electrons with the Scanning Tunneling Microscope, Phys. Rev. Lett. **65**, 247 (1990).

[76] Z. Lenac, M. Sunjić, H. Conrad, and M. E. Kordesch, Image-potential states on clean and hydrogen-covered Pd surfaces: Analysis of a one-dimensional model, Phys. Rev. B **36**, 9500 (1987).

[77] C. T. Chen and N. V. Smith, Unoccupied surface states on clean and oxygen-covered Cu (110) and Cu (111), Phys. Rev. B **40**, 7487 (1989).

[78] M. Ormaza, R. Robles, N. Bachellier, P. Abufager, N. Lorente, and L. Limot, On-surface engineering of a magnetic organometallic nanowire, Nano Lett. **16**, 588 (2015).

[79] H. Oka, K. Tao, S. Wedekind, G. Rodary, V. S. Stepanyuk, D. Sander, and J. Kirschner, Spatially Modulated Tunnel Magnetoresistance on the Nanoscale, Phys. Rev. Lett. **107**, 187201 (2011).